This is the accepted manuscript made available via CHORUS. The article has been published as:

Strength, hardness, and lattice vibrations of Z-carbon and W-carbon: First-principles calculations

Zhiping Li, Faming Gao, and Ziming Xu

Phys. Rev. B **85**, 144115 — Published 23 April 2012

DOI: 10.1103/PhysRevB.85.144115

Strength, hardness and lattice vibrations of *Z*-carbon and *W*-carbon: First-principles calculations

Zhiping Li, Faming Gao*, Ziming Xu
Key Laboratory of Applied Chemistry, Yanshan University, Hebei Qinhuangdao 066004, China

The strength, hardness and lattice vibrations of two novel superhard carbon allotropies, *Z*-carbon and *W*-carbon are investigated by first-principle calculations. Phonon dispersion calculations indicate that *Z*-carbon and *W*-carbon are dynamically stable at least up to 300 GPa. The strength calculations reveal that the failure mode in *Z*-carbon is dominated by the tensile type and the [010] direction is the weakest one. In *W*-carbon the failure mode is dominated by the shear type and the $(101)[11\bar{1}]$ direction is the weakest one. Although the ideal strength of diamond are distinctly greater than that of *Z*-carbon and *W*-carbon, the tensile strength and shear strength for Z-carbon and *W*-carbon show much lower anisotropy than that of diamond. The hardness calculations indicate that the average hardness of *Z*-carbon is less than that of diamond, but greater than that of the *W*-carbon, *M*-carbon and bct-C_4 carbon. The simulated Raman spectra show that the A_g modes at 1094 cm^{-1} for *Z*-carbon and 1109.7 cm^{-1} for *W*-carbon are in agreement with that of 1082 cm^{-1} observed in the experiment of cold-compressed graphite at 9.8 GPa.

PACS numbers: 62.20.-x, 71.15.Mb, 81.05.Zx

* Electronic address:fmgao@ysu.edu.cn

I. INTRODUCTION

Owing to its flexibility of bond hybridization, the element carbon can exist in various forms, such as graphite, fullerenes, nanotubes, diamond. The cubic diamond is the hardest phase as known at present. Since the superhard materials show the significant applications in industry, scientists expect to find a new carbon phase with hardness exceeding that of diamond. The extensive theoretical[1–3] and experimental[4] studies have been carried out over the past decades. Using high pressure technique, Mao et al.[4] and Kumar et al.[5] obtained respectively new carbon phases which all left a ring crack indentation on the diamond anvils. However, this phase cannot quench to room temperature, rendering it difficult to determine the details about the atomistic structure and related physical properties. Recently, an efficient and reliable methodology for crystal structure prediction, ab initio evolutionary algorithm method[6-8], was developed. And a monoclinic *C*2/m phase (*M*-carbon) was predicted,[6, 9] which show a good match with the experimental XRD patterns for such cold-compressed graphite.[4, 9] More recently, the body-centered tetragonal bct-C_4 carbon,[10,13,14,15] orthorhombic *W*-carbon[11] and *Z*-carbon[12] were also proposed. *M*-carbon is stable over cold-compressed graphite above 13.4 GPa, whereas bct-C_4 carbon is stable above 20 GPa. Due to the similarity of their structures, these phases could coexist in high pressure experiments. Although the structures of these phases are determined in theory,[6-9] the mechanical properties and vibrational properties (Raman and IR spectra) of *Z*-carbon and *W*-carbon remain large unexplored. In this work, we perform first-principles calculations to investigate the vibrational properties, ideal strength and theoretical hardness of two novel carbon allotropies, *Z* and *W* carbon. For comparison, *M*-carbon and bct-C_4 carbon[10] are also calculated. Elastic calculations demonstrate that they are mechanically stable. Phonon dispersion indicates that *Z* and *W* carbon are dynamically stable at least up to 300 GPa. Ideal strength demonstrates that the lowest peak shear stress for *Z*-carbon is higher than *W*-carbon, *M*-carbon and bct-C_4 carbon. The detailed calculations for their hardness are also performed on atomic scale, which help to understand why a ring scratch indentation left on diamond anvils in Mao' s and Kumar's experiments.

II. Computational details

The ground-state, elastic properties and ideal strength are calculated using the projector augmented-wave method[16] employed to describe the electron-ion interaction within density functional theory(DFT), [17, 18] as implemented in the Vienna ab initio simulation package (VASP).[16, 19] For the

exchange and correlation functional, the general gradient approximation (GGA) of the Perdew Burke Ernzerhof (PBE) parameterization[20] was used. Integrations over the Brillouin zone were performed using Monkhorst-Pack (use a tetrahedron method for BZ integration） grids.[21] The number of k-points sampling in the Brillouin zone was 0.25 $Å^{-1}$ for unit cell and the plane-wave cutoff energy was set to 550 eV tested to ensure that the total energies converged to 1meV per atom. Optimization of structural parameters was achieved by the minimization of forces and stress tensors. The elastic constants were determined by applying an appropriate set of distortions with the distortion parameter δ varying between −0.02 and +0.02. Calculations of the lattice vibrations were carried out using the density functional perturbation theory (DFPT)[22] within the local density approximation[17] in a plane wave basis, as implemented in the Quantum ESPRESSO code[23] with the Troullier–Martins (TM) pseudopotentials[24] prepared by the Fritz Haber Institute code[25] and taken from the Abinit web page[26]. The plane wave cutoff energy of 110 Ry is used in the calculations and the estimated energy error in self-consistency was less than 10^{-14} a.u. The calculations of stress-strain relations were performed by the method of Refs. 27 and 28. This approach with a relaxed loading path has been successfully applied to the calculation of the strength of several strong solids.[29-31]. Hardness calculations are based on a micro hardness models for covalent crystal.[32-36]

III. RESULT

A. Elastic stabilities, incompressibility, and rigidity

The calculated lattice constants for the equilibrium structure of *Z*-carbon and *W*-carbon with GGA are listed in Table I. For comparison, the calculated results of *M*-carbon and bct-C_4 carbon are also listed in Table I. The computed lattice parameters for *Z*-carbon and *W*-carbon with GGA method are in a good agreement with the available theoretical data. *Z*-carbon forms in an orthorhombic lattice (space group *Cmmm*, No. 65) with sixteen carbon atoms per unite cell. The relaxed lattice parameters with GGA functional are *a*=8.771 Å, *b*=4.255 Å, *c*=2.515 Å, which are in excellent agreement with Amsler's result,[9] differing only by 1.2%, 1.1% and 1.2%, respectively. *W*-carbon forms in an orthorhombic lattice (space group *Pnma*, No. 62) with sixteen carbon atoms per unit cell. Its relaxed lattice parameters with GGA functional are *a* =9.084 Å, *b* =2.525 Å, *c*=4.156 Å, which are in excellent agreement with Wang's results,[8] differing only by 1.2%, 1.2% and 1.0%, respectively. The agreement of our calculated structural parameters with the published results shows the accuracy and reliability of our calculations.

We will examine mechanical stability of *W*-carbon and *Z*-carbon by calculation of single-crystal zero-pressure elastic constants. The elastic coefficients were determined by applying a set of given homogeneous deformations with a finite value and calculating the resulting energy with respect to optimizing the internal atomic freedoms implemented by Patil et al.[37] The structural stability of

M-carbon, bct-C_4 carbon and diamond are also investigated by calculating elastic coefficients using the approach represented in Ref, 38 and 37. The calculated results are listed in Table I. Our calculated elastic constants (C_{11}, C_{12}, and C_{44}) of diamond by GGA are in reasonable agreement with a previous experiment of McSkimin.[40] To achieve mechanical stability, the elastic constants of the crystal should satisfy the generalized elastic stability criteria. For a stable orthorhombic structure, its nine independent elastic constants C_{ij} (C_{11}, C_{22}, C_{33}, C_{44}, C_{55}, C_{66}, C_{12}, C_{13} and C_{23} in Voigt notation) should satisfy the well-known Born stability criteria,[41] i.e., ($C_{11}>0$, $C_{22}>0$, $C_{33}>0$, $C_{44}>0$, $C_{55}>0$, $C_{66}>0$, $[C_{11}+C_{22}+C_{33}+2(C_{12}+C_{13}+C_{23})]>0$, $(C_{11}+C_{22}-2C_{12})>0$, $(C_{11}+C_{33}-2C_{13})>0$, and $(C_{22}+C_{33}-2C_{23})>0$. Clearly, these calculated elastic constants C_{ij} satisfy the Born stability criteria, suggesting that the orthorhombic phases of *Z*-carbon and *W*-carbon are elastic stability at ambient conditions.

On the basis of the Voigt-Reuss-Hill approximation,[42] we have calculated the corresponding bulk and shear moduli from the single crystal zero-pressure elastic constants, which may be determined on the polycrystalline samples experimentally. For specific cases of orthorhombic lattices, the Reuss bulk modulus (B_R) and the Voigt bulk modulus (B_V) are given by

$B_V=1/9[C_{11}+C_{22}+C_{33}+2(C_{12}+C_{13}+C_{23})]$

$B_R=\Delta[C_{11}(C_{22}+C_{33}-2C_{23})+C_{22}(C_{33}-2C_{13})-2C_{33}C_{12}+C_{12}(2C_{23}-C_{12})+C_{13}(2C_{12}-C_{13})+C_{23}(2C_{13}-C_{23})]^{-1}$

and the Ruess shear modulus (G_R) and the Voigt bulk modulus (G_V) are defined as

$G_V=1/15[C_{11}+C_{22}+C_{33}+3(C_{44}+C_{55}+C_{66})-(C_{12}+C_{13}+C_{23})]$

$G_R=15\{4[C_{11}(C_{22}+C_{33}+C_{23})+C_{22}(C_{33}+C_{13})+C_{33}C_{12}-C_{12}(C_{23}+C_{12})-C_{13}(C_{12}+C_{13})-C_{23}(C_{13}+C_{23})]/\Delta+3[(1/C_{44})+(1/C_{55})+(1/C_{66})]\}^{-1}$

where $\Delta=C_{13}(C_{12}C_{23}-C_{13}C_{22})+C_{23}(C_{12}C_{13}-C_{23}C_{11})+C_{33}(C_{11}C_{22}-C_{12}^2)$

Additionally, the Young modulus and Poisson's ratio are calculated, as presented in Table II. The elastic constants, bulk and shear modulus of *M*-carbon, bct-C_4 carbon and diamond are also calculated to compare with *Z*-carbon and *W*-carbon, as presented in Table I and II. Our results demonstrate that the values of the bulk and shear modulus for Z-carbon, *W*-carbon, *M*-carbon and bct-C_4 carbon are all above 400 GPa, indicating the four carbon allotropes are all the potential low compressible materials. Considering that the bulk modulus can be as a measure of the average bond strength and the shear modulus can be as a measure of the resistance to a change in bond angle by an external force, Tanaka et al.[44] proposed that G/B represents the relative directionality of the bonding in the material. For those carbon phases, the calculated ratio of G_0/B_0 in rang from 1.04 to 1.15 is slightly smaller than 1.19 of diamond, which indicates that the directionality of the bonding is strong. Moreover, the brittleness and ductility can be estimated by the Frantsevich rule[45]. It is clearly seen from Table II that bct-C_4 carbon posses a much better ductility than diamond. The rigidity for *Z*-carbon is most close to diamond among

the four new carbon phases.

B. Stress-strain response in tension and shear

To understand the strength under plastic deformation at the atomic level occurs by permanent large strain, we carried out the calculations of ideal strength within GGA scheme. Fig. 1(*a*) shows that the stress-strain relation in <100>, <110>, and <111> directions for diamond. Fig. 1 (*b*) shows that the stress-strain relation in *x*, *y*, and *z* of the Cartesian axes directions for *M*-carbon. Fig. 1 (*c*) shows that the stress-strain relation in [100], [001], [110], [011], and [111] directions for bct-C_4 carbon. Our calculated results for the tensile strength of diamond are 203.9, 115.6, and 83.8 GPa in (100), (110), and (111) directions, respectively. The calculate tensile strength of *M*-carbon are 83.4, 110.8, and 115.5 GPa in *x*, *y*, and *z* axis directions, respectively. The calculated tensile strength for bct-C_4 carbon in [100] and [001] directions are 78.9 and 129.2 GPa, respectively. These results are in excellent agreement with those of previous calculations.[29]

The stress-strain relations of *Z*-carbon and *W*-carbon in principle symmetry directions are systematically examined under tensile loading. The stress-strain curves for *Z*-carbon and *W*-carbon are presented in Fig. 1(*d*) and (*e*). As shown in Fig. 1(*d*), *Z*-carbon has strong stress responses in the [100], [010], [001], [110], [011], [101] and [111] directions with the peak tensile stresses between 70 and 130 GPa. As shown in Fig. 1(*e*), *W*-carbon has strong stress responses in the above directions with the peak tensile stresses between 70 and 120 GPa. For *Z*-carbon, the highest peak stress in the [001] direction is about 127.5 GPa, which is higher than the highest tensile strength of *W*-carbon. For *W*-carbon, the peak stress in the [001] and [010] directions are about 112.7 and 110.8 GPa, respectively, which are evidently larger than that of the other principal symmetry directions. The lowest peak tensile stress for *W*-carbon is 68.8 GPa in the [101] direction. The calculated anisotropic ideal tensile strengths for *Z*-carbon and *W*-carbon are listed in Table IV. The anisotropy ratio of ideal tensile strengths for *Z*-carbon is $\sigma_{[001]}$: $\sigma_{[111]}$: $\sigma_{[110]}$: $\sigma_{[101]}$: $\sigma_{[100]}$: $\sigma_{[011]}$: $\sigma_{[010]}$ ≈ 1.79: 1.43: 1.37: 1.35: 1.28: 1.21: 1. The anisotropy ratio of ideal tensile strengths for *W*-carbon is $\sigma_{[001]}$: $\sigma_{[010]}$: $\sigma_{[011]}$: $\sigma_{[110]}$: $\sigma_{[100]}$: $\sigma_{[111]}$: $\sigma_{[101]}$≈ 1.64: 1.61: 1.42: 1.26: 1.22: 1.05: 1. The anisotropy ratio of ideal tensile strengths of *Z*-carbon and *W*-carbon are smaller than that of diamond($\sigma_{[100]}$=203.9 GPa : $\sigma_{[110]}$=115.6 GPa : $\sigma_{[111]}$=83.8 GPa≈ 2.43 : 1.38 : 1). The anisotropy of tensile strength for *Z* and *W*-carbon are much lower than diamond. These reductions of the tensile strength anisotropy result from the directional arrangements of bonds in *Z*-carbon and *W*-carbon. The direction of the weakest tensile strength in *Z*-carbon and *W*-carbon is [010]

and [101] with the lowest peak stress of 71.4 GPa and 68.8 GPa, respectively, which is smaller than the weakest tensile strength of 83.8 GPa for diamond in <111> direction.

. We also make a comprehensive study on the stress-strain relations of *Z*-carbon and *W*-carbon in various symmetry directions under shear deformation. The calculated stress-strain curves along principle shear paths in *Z*-carbon and *W*-carbon are shown in Fig. 2(*a*) and (*b*), respectively. The highest shear strength of 109.3 GPa is found under the (001)[100] shear loading for *Z*-carbon, and of 100.7 GPa under the (101)[010] shear loading for *W*-carbon, respectively. These values are slightly higher than the highest shear strength of 94 GPa for M-carbon and 96.7 GPa for bct-C_4 carbon as shown in Fig 2. The calculated anisotropic ideal shear strengths for *Z*-carbon and *W*-carbon are shown in Table V. The anisotropy ratio of ideal shear strengths for *Z*-carbon is $\sigma_{(001)[100]}$: $\sigma_{(001)[110]}$: $\sigma_{(001)[010]}$: $\sigma_{(100)[001]}$: $\sigma_{(100)[011]}$: $\sigma_{(010)[001]}$: $\sigma_{(100)[010]}$: $\sigma_{(010)[101]}$: $\sigma_{(010)[100]}$ ≈ 1.25: 1.25: 1.2: 1.18: 1.45: 1.45: 1.07:1: 1. The anisotropy ratio of ideal shear strengths for *W*-carbon is $\sigma_{(101)[010]}$: $\sigma_{(100)[010]}$: $\sigma_{(001)[010]}$: $\sigma_{(001)[110]}$: $\sigma_{(001)[100]}$: $\sigma_{(100)[011]}$: $\sigma_{(100)[001]}$: $\sigma_{(101)[10\bar{1}]}$: $\sigma_{(101)[11\bar{1}]}$≈ 1.62: 1.56: 1.45: 1.34: 1.22: 1.17: 1.09: 1.03: 1. The anisotropy ratio of *Z*-carbon is significant smaller than *W*-carbon and diamond ($\sigma_{(111)[\bar{1}\bar{1}2]}$=130 GPa : $\sigma_{(111)[\bar{1}\bar{1}2][1\bar{1}0]}$=100.6 GPa : $\sigma_{(111)[11\bar{2}]}$=91 GPa≈1.43 : 1.11 : 1). It is found that the weakest shear strength of 87.2 GPa at strain of 0.28 in (010)[100] direction is higher than the weakest tensile strength of 71.4 GPa at strain of 0.12 in [010] direction as much as 22% for *Z*-carbon. Simultaneously, it is found that the weakest shear strength of 62.1 GPa at strain of 0.16 in (101)[$11\bar{1}$] direction is lower than the weakest tensile strength of 68.8 GPa at strain of 0.13 in [101] direction as much as 9.7% for *W*-carbon. Hence, the failure mode in *Z*-carbon is dominated by the tensile type in [010] direction. In *W*-carbon it is dominated by the shear type in (101)[$11\bar{1}$] direction. To understand this intriguing bond breaking pattern, we have calculated the electron localization function (ELF)[46-47] that enables an effective and reliable analysis of the nature and extent of covalent bonding. The instability of C-C bonds under shear deformation for *Z* and *W* carbon polymorphs can be attributed to a local transformation of sp^3 to sp^2 upon the shear. The inhomogeneous weakening of three-dimensional C-C bonds shown in both carbon polymorphs can also be correlated to the significantly electronic fluctuation as seen in the ELF map in Fig. 3. Moreover, The highest shear strength in the (010) easy slip plane is found to be 99.9 GPa under the (010)[001] shear loading for *Z*-carbon and in the (101) easy slip plane is found to be 100.7 GPa under the (101)[010] shear loading for *W*-carbon, respectively, which is suggested as a dominant role in resisting a indenter.[48]

C. Hardness calculations

According to the microscopic hardness model,[32-36] the atomic bond hardness for *Z*-carbon and *W*-carbon are calculated, which is an essential factor to determine the magnitude of the peak stress in shear direction when a crystal under indenter.

The hardness of the carbon allotropes are shown in TABLE III. The calculated average hardness of *Z*-carbon, *W*-carbon, *M*-carbon and bct-C_4 carbon are slightly less than that of diamond. *Z*-carbon is harder than *W*-carbon, *M*-carbon and bct-C_4 carbon. Especially, the C-C bonds connected the carbon squares (Fig. 4(*a*)) in *Z*-carbon, denoted by red lines in Fig. 4(*b*), show high hardness,108 GPa, about 16.14% higher than that of diamond. To understand the high bonding hardness in *Z*-carbon, we also calculated the electron localization functions (ELF) to distinguish different bonding interactions in *Z*-carbon. The structure with ELF isosurfaces for *Z*-carbon is presented in Fig. 5(*a*). The isosurface plots at ELF = 0.75 (a typical number for characterization of covalent bonding)[49] clearly illustrate the nature of strong covalent bonding in *Z*-carbon. Moreover, a greater amount of charge localized in the C-C bonding regions connected carbon squares, indicating a strong covalent interaction. Similarly, the structure with ELF isosurfaces for *W*-carbon is presented in Fig. 5(*b*) with bond hardness labeled.

D. Lattice vibrations

The computed phonon dispersion curves (left panel) and density of states (right panel) of *Z*-carbon and *W*-carbon are represented in Fig. 6 (*a*) and (*b*), respectively. No imaginary frequencies were observed throughout the whole Brillioun zone, confirming dynamical stability of the orthorhombic *Z*-carbon and *W*-carbon at least up to 300 GPa. Vibrational spectroscopy for *Z*-carbon, *W*-carbon and the other two carbon allotropes of *W*-carbon and bct-C_4 carbon are studied to identify the possible phases in cold compressive graphite. The frequencies, symmetry species for the vibrational modes with Raman optical activity of *Z*-carbon, *W*-carbon, *M*-carbon and bct-C_4 carbon are represented in Table VI. A primitive cell for *Z*-carbon with eight atoms is used in the calculations. In as much as the primitive cell of *Z*-carbon containing eight atoms, there should be twenty-four phonon modes at Γ point, including three acoustic modes and twenty-one optical modes respectively. The orthorhombic unit cell of *W*-carbon containing sixteen atoms, there should be forty-eight phonon modes at Γ point, including three acoustic modes and forty-five optical modes respectively. The factor group analysis at the Γ point yields twelve optical modes irreducible representations with Raman activity for *Z*-carbon, as listed in

Table VI. For *Z*-carbon, the three modes with strong Raman peak could be detected at 1063.0, 1194.2 and 1328.5 cm^{-1}, the relative weak peaks are located at 987.7, 1259.5 and 1300.6 cm^{-1}, and the others are too weak to be found, as shown in Fig. 7(*a*). For *W*-carbon, there are twenty-four optical modes irreducible representations with Raman activity as shown in Table VI. The eleven strong Raman peaks are located at 909.5, 1087.8, 1133.8, 1243.7, 1253.0, 1258.5, 1270.4, 1285.5, 1294.7, 1346.6 and 1398.7 cm^{-1} and the three relative weak peak are located at 1002.0, 1195.4 and 1238.1 cm^{-1}(Fig. 7(*b*)). For the other two carbon allotropes, the characteristic Raman peaks are found located at 881.1, 917.3, 1005.2, 1137.7, 1222.0, 1248.1, 1255.9, 1279.2, 1318.7 , 1341.8 and 1414.7 cm^{-1} for *M*-carbon(Fig. 7(*c*)), and 1086.6 and 1350.5 cm^{-1} for bct-C_4 carbon(Fig. 7(*d*)), respectively. For a more clearily compare to the availible expermental data, the vibrational spectroscopy for those carbon allotropes at 9.8 GPa and 15.2 GPa are simulated respectively. The Raman peak located at 1063.3 cm^{-1} with A_g symmetry for *Z*-carbon are located at 1093.5 cm^{-1} at pressure of 9.8 GPa and 1112.1 cm^{-1} at pressure of 15.2 GPa, respectively, which are in agreement with the experimental results of a clear Raman peak appears at 1082 cm^{-1} at pressure of 9.8 GPa and 1094 cm^{-1} at pressure of 15.2 GPa obtained by the high pressure Raman measurements for the cold-compressed graphite.[12] For *W*-carbon, the peaks located at 1109.7 cm^{-1} at 9.8 GPa and 1121.8 cm^{-1} at 15.2 GPa. For *M*-carbon, the peaks located at 1167.8 cm^{-1} at 9.8 GPa and 1184.6 cm^{-1} at 15.2 GPa. For bct-C_4 carbon, the peaks located at 1108.6 cm^{-1} at 9.8 GPa and 1119.6 cm^{-1} at 15.2 GPa, respectively.

To provide a more precise characterization for the possible phase existed in the cold compressive graphtie, the IR spectra for those carbon allotropes are simulated. The frequencies, symmetry species for the vibrational modes with infrared optical activity of *Z*-carbon, *W*-carbon, *M*-carbon and bct-C_4 carbon are represented in Table VII. The infrared absorption spectra are shown in Fig. 8. There are strong absorption modes at 988.3 and 1010.5 cm^{-1} for *Z*-carbon, 668.6, 945.9, 1062.1, 1102.7, 1141.5, 1268.6, 1280.9 and 1299.3 cm^{-1} for *W*-carbon, 668.4, 938.2, 1118.6, 1148.3 and 1282.5 cm^{-1} for *M*-carbon, and 1016.7 cm^{-1} for bct-C_4 carbon. The peaks of 945.9 cm^{-1} for *W*-carbon and 938.2 cm^{-1} for *M*-carbon approach the peak of 988.3 cm^{-1} for Z-carbon. The peak of 1016.7 cm^{-1} of bct-C_4 carbon approaches the peak of 1010.5 cm^{-1} for Z-carbon. The structure of *M*-carbon contains five-, six- and seven-membered rings, with alternating zigzag and armchair buckled carbon sheets via a one-layer by three-layer slip mechanism, similar to *W*-carbon. The structure of *Z*-carbon contains four-, six- and eight-membered rings, can be interpreted as a combination of hexagonal diamond and bct-C_4 carbon.[14] The structural analogy between the M and W phases results in a very similar IR spectra. Their

characteristic infrared peaks are more than *Z*-carbon and bct-C_4 carbon, as shown in Fig. 8.

V. CONCLUSIONS

The comprehensive studies about the structural, elastic, lattice vibrations, anisotropic ideal strength of *Z*-carbon and *W*-carbon have been performed by first principles. Elastic constants and phonon dispersions demonstrate that *Z*-carbon and *W*-carbon are structurally stable. The simulated Raman spectra located at 1093.5 cm^{-1} for *Z*-carbon and 1109.7 cm^{-1} for *W*-carbon approach the peak of 1082 cm^{-1} obtained experimentally from the cold-compressed graphite at 9.8 GPa. The tensile and shear strength and hardness calculations indicate that *Z*-carbon and *W*-carbon possess the superior mechanical properties. And they are the potential superhard materials.

Acknowledgements

Financial support from the National Natural Science Foundation of China (Grant No.21071122, 21101134) and Research Fund for the Doctoral Program of Higher Education of China (Grant No.20091333110009) and the Natural Science Foundation of Hebei (Grant No. ZD2010112, E2010001169, QHD-201101A130).

[1] A.Y. Liu and M. L. Cohen, Science **245**, 841 (1989).

[2] D. M. Teter and R. J. Hemley, Science **271**, 53 (1996).

[3] R. B. Kaner, J. J. Gilman, and S. H. Tolbert, Science **308**, 1268 (2005).

[4] W. L. Mao, H.-K. Mao, P. J. Eng, T. P. Trainor, M. Newville, C.-C Kao, D. L. Heinz, J. Shu, Y. Meng, and R. J. Hemley, Science **302**, 425 (2003).

[5] R. S. Kumar, M. G. Pravica, A. L. Cornelius, M. F. Nicol, M. Y. Hu, and P. C. Chow, Diam. Relat. Mater. **16**, 1250 (2007).

[6] A. R. Oganov and C. W. Glass, J. Chem. Phys. **124**, 244704 (2006).

[7] A. R. Oganov, A. O. Lyakhov, and M Valle, Acc. Chem. Res. **44**, 227 (2011).

[8] A. R. Oganov, J. H. Chen, C. Gatti, Y. Z. Ma, Y. M. Ma, C. W. Glass, Z. X. Liu, T. Yu, O. O. Kurakevych, and V. L. Solozhenko, Nature **457**, 863, (2009).

[9] Q. Li, Y. M. Ma, A. R. Oganov, H. B. Wang, H. Wang, Y. Xu, T. Cui, H.-K. Mao, and G. T. Zou, Phys. Rev. Lett. 102, 175506 (2009).

[10] K. Umemoto, R. M. Wentzcovitch, S. Saito, and T. Miyake, Phys. Rev. Lett. **104**, 125504 (2010).

[11] J. T. Wang, C. F. Chen, and Y. Kawazoe. Phys. Rev. Lett. **106**, 075501 (2011).

[12] M. Amsler, J. A. Flores-Livas, L. Lehtovaara, F. Balima, S. A. Ghasemi, D. Machon, S. Pailhès, A. Willand, D. Caliste, S. Botti, A. S. Miguel, S. Goedecker, and M. A. L. Marques, Phys. Rev. Lett. **108**, 065501 (2012).

[13] R. H. Baughman and D.S. Galvlo. Chem. Phys. Lett. **211**, 110 (1993).

[14] R. H. Baughman, A. Y. Liu, C. Cui, and P. J. Schields. Synth. Met. **86**, 2371 (1997) .

[15] Y. Omata, Y. Yamagami, K. Tadano, T. Miyake, and S. Saito. Physica E. **29**, 454 (2005).

[16] G. Kresse and D. Joubert, Phys. Rev. B **59,** 1758 (1999).

[17] P. Hohenberg and W. Kohn, Phys. Rev. **136,** B864 (1964).

[18] W. Kohn and L.J. Sham, Phys. Rev. **140**, A1133 (1965).

[19] G. Kresse and J. Furthmuller, Phys. Rev. B **54,** 11169(1996).

[20] J. P. Perdew, K. Burke, and M. Ernzerhof, Phys. Rev. Lett. **77**, 3865 (1996).

[21] H. J. Monkhorst and J. D. Pack, Phys. Rev. B **13**, 5188 (1976).

[22] S. Baroni, S. de Gironcoli, A. Dal Corso, and P. Giannozzi, Rev. Mod. Phys. **73**, 515 (2001).

[23] P. Giannozzi, S. Baroni, N. Bonini, M. Calandra, R. Car, C. Cavazzoni, D. Ceresoli, G. L. Chiarotti, M. Cococcioni, I. Dabo, A. Dal Corso, S. de Gironcoli, S. Fabris, G. Fratesi, R. Gebauer, U. Gerstmann, C. Gougoussis, A. Kokalj, M. Lazzeri, L. Martin-Samos, N. Marzari, F. Mauri, R. Mazzarello, S. Paolini, A. Pasquarello, L. Paulatto, C. Sbraccia, S. Scandolo, G. Sclauzero, A. P. Seitsonen, A. Smogunov, P. Umari, and R. M. Wentzcovitch, J. Phys.: Condens. Matter

21, 395502 (2009); http://www.quantum-espresso.org.

[24] N. Troullier, J. L. Martins, Phys. Rev. B **43,** 1993 (1991).

[25] M. Fuchs, M. Scheffler, Comput. Phys. Commun. **119,** 67 (1999).

[26] X. Gonze, J.-M. Beuken, R. Caracas, F. Detraux, M. Fuchs, G.-M. Rignanese, L. Sindic,M. Verstraete, G. Zerah, F. Jollet,M. Torrent, A. Roy, M. Mikami, Ph. Ghosez, J.-Y. Raty, and D. C. Allan, Comput. Mat. Sci. **25**, 478 (2002); http://www.abinit.org.

[27] D. Roundy, C. R. Krenn, Marvin L. Cohen, and J. W. Morris, Jr., Philos. Mag. A **81**, 1725 (2001).

[28] D. Roundy, C. R. Krenn, Marvin L. Cohen, and J. W. Morris, Jr., Phys. Rev. Lett. **82**, 2713 (1999).

[29] R. F. Zhang, Z. J. Lin, and S. Veprek, Phys. Rev. B **83**, 155452 (2011).

[30] R. F. Zhang, Z. J. Lin, H.-K. Mao, and Y. S. Zhao, Phys. Rev. B **83**, 060101(R) (2011).

[31] Y. Zhang, H. Sun, and C. F. Chen, Phys. Rev. Lett. **93**, 195504 (2004); **94**, 145505 (2005).

[32] F. M. Gao, J. L. He, E. D. Wu, S. M. Liu, D. L. Yu, D. C. Li, S. Y. Zhang, and Y. J. Tian, Phys. Rev. Lett. **91**, 015502 (2003).

[33] F. M. Gao and L. H. Gao, J. Superhard Mater. **32**, 148 (2010).

[34] F. M. Gao, Phys. Rev. B **73**, 132104 (2006).

[35] Z. P. Li and F. M. Gao, Phys. Chem. Chem. Phys. **14,** 869, (2012).

[36] Y. H. Xu, F. M. Gao, and X. F. Hao, Phys. Status Sol., RRL, **4**, 200 (2010).

[37] S. K. R. Patil, S. V. Khare, B. R. Tuttle, J. K. Bording, and S. Kodambaka, Phys. Rev. B **73**, 104118 (2006).

[38] P. Söderlind and J. E. Klepeis, Phys. Rev. B **79**, 104110 (2009).

[39] X.-Q. Chen, C. L. Fu, and R. Podloucky, Phys. Rev. B **77**, 064103 (2008).

[40] H. J. McSkimin and P. Andreatch, J. Appl. Phys. **43**, 985 (1972).

[41] Z. J. Wu, E. J. Zhao, H. P. Xiang, X. F. Hao, X. J. Liu, and J. Meng, Phy. Rev. B **76**, 054115 (2007).

[42] R. Hill, Proc. Phys. Soc. London **65**, 349 (1952).

[43] H. Y. Niu, P. Y. Wei, Y Sun, X.-Q. Chen, C. Franchini, D. Z. Li, and Y. Y. Li, Appl. Phys. Lett. **99**, 031901 (2011).

[44] K. Tanaka, K. Okamoto, H. Inui, Y. Minonishi, M. Yamaguchi, and M. Koiwa, Philos. Mag. A **73**, 1475 (1996).

[45] I. N. Frantsevich, F. F. Voronov, and S. A. Bokuta, *Elastic Constants and Elastic Moduli of Metals and Inslators*: Handbook (Naukova Dumka, Kiev, 1982).

[46] B. Silvi and A. Savin, Nature **371**, 683 (1994).

[47] A. D. Becke and K. E. Edgecombe, J. Chem. Phys. **92**, 5397 (1990).

[48] J. Yang, H. Sun, and C. F Chen, J. Amer. Chem. Soc. **130**, 7200 (2008).

[49]A. Savin, R. Nesper, S. Wengert, and T. F. Fässler, Angew. Chem., Int. Ed. Engl. **36**, 1808 (1997).

Table I. Calculated equilibrium lattice parameters, a(Å), b(Å), c(Å), β(°), equilibrium volume V_0(Å^3/atom), zero-pressure elastic constants C_{ij}(GPa), and density ρ(g/cm^3), and total energy E_0 (eV/atom) of Z-carbon and W-carbon, compared with available data of M-carbon, bct-C_4 carbon and diamond.

Phase	Z-carbon	W-carbon	M-carbon	bct-C_4	diamond	
	Present work	Present work	Present work	Present work	Present work	Calc/Expt
V_0	5.865	5.957	5.974	6.022	5.702	
a	8.771	9.084	9.193	4.38	3.573	
b	4.255	2.525	2.525			
c	2.514	4.516	4.149	2.511		
β			97.029			
C_{11}	1070.6	890.2	929.5	930.3	1051.1	1067 [a] /1079 [b]
C_{22}	1102.6	1084.9	1087.0			
C_{33}	1184.5	1045.2	1044.2	1189.9		
C_{44}	452.3	523.6	521.0	446.6	560.6	571 [a] /578 [b]
C_{55}	500.6	459.1	451.7			
C_{66}	363.4	388.9	388.5	320.6		
C_{12}	76.9	51.8	48.6	173.8	127.7	132 [a] /124 [b]
C_{13}	89.7	162.0	156.3	59.8		
C_{23}	-1.2	85.1	86.9			
C_{15}			62.9			
C_{25}			-28.2			
C_{35}			25.6			
C_{46}			-7.8			
ρ	3.401	3.348	3.339	3.312	3.498	
E_0	-8.961	-8.936	-8.928	-8.893	-8.965	

[a] Reference 39

[b] Reference 40

Table II. Calculated isotropic bulk modulus B_0 (GPa), shear modulus G_0 (GPa), ratio of G_0/B_0, Young's modulus E (GPa), and Poisson's ratio υ for orthorhombic *Z*-carbon and *W*-carbon compared to those of *M*-carbon, bct-C_4 carbon and diamond at ambient pressure.

Phase	*Z*-carbon		*W*-carbon		*M*-carbon		bct-C_4		diamond	
	Present work	Calc	Present work	Calc	Present work	Calc	Present work	Calc	Present work	Calc/Expt
G_R	465.4		448.4		451.0		413.2		516.4	
G_V	476.1		455.7		456.8		426.6		521	
$G_0=(G_R+G_V)/2$	470.7		452.1	451 [b]	453.9	446 [b]	419.9	421 [c]	518.7	527 [d] /538 [e]
B_R	409.4		399.5		402.3		402.7		435.1	
B_V	409.8		402.0		404.9		404.1		435.1	
$B_0=(B_R+B_V)/2$	409.6	441.5 [a]	400.8	403 [b]	403.6	400 [b]	403.4	404 [c]	435.1	444 [d] /443 [e]
G_0/B_0	1.15		1.13		1.12		1.04		1.19	
E_H	1021.1		985.6		990.4		935.3		1113.8	
υ	0.08		0.09		0.09		0.11		0.07	

[a] Reference 12

[b] Reference 43

[c] Reference 36

[d] Reference 39

[e] Reference 40

Table III. Calculated bonds and average hardness for *Z*-carbon and *W*-carbon compared to those of *M* -carbon, bct-C_4 carbon and diamond.

Phase	Bond type (numbers)	d_μ (Å)	v_b^μ (Å^3)	P_{AB}	N_e^μ (Å^{-3})	H_v^μ (GPa)	$H_{v\,av.}$ (GPa)
Z-carbon	C-C (16)	1.533	2.831	0.885	0.848	107.952	90.23
	C-C (4)	1.563	3.004	0.71	0.618	83.231	
	C-C (4)	1.564	3.010	0.62	0.559	77.661	
	C-C (4)	1.570	3.043	0.56	0.499	71.412	
	C-C (4)	1.576	3.079	0.58	0.492	70.074	
W-carbon	C-C (4)	1.506	2.714	0.7	0.647	94.232	89.54
	C-C (4)	1.521	2.800	0.89	0.797	105.536	
	C-C (4)	1.536	2.880	0.885	0.771	100.809	
	C-C (8)	1.557	3.000	0.71	0.615	83.821	
	C-C (8)	1.573	3.096	0.83	0.696	88.727	
	C-C (4)	1.598	3.244	0.71	0.568	74.531	
M-carbon	C-C (4)	1.503	2.707	0.71	0.658	95.684	89.25
	C-C (4)	1.522	2.811	0.89	0.794	105.106	
	C-C (4)	1.531	2.861	0.885	0.776	101.968	
	C-C (2)	1.538	2.901	0.69	0.622	86.987	
	C-C (4)	1.542	2.920	0.72	0.640	88.222	
	C-C (2)	1.561	3.032	0.72	0.617	83.376	
	C-C (8)	1.573	3.101	0.83	0.695	88.627	
	C-C (4)	1.626	3.426	0.7	0.512	66.549	
bct-C_4	C-C (4)	1.524	2.852	0.92	0.878	112.001	87.17
	C-C (4)	1.579	3.170	0.55	0.472	67.840	
diamond	C-C (4)	1.547	2.851	0.75	0.702	92.949	92.95

Table IV. Calculated ideal tensile strength for *Z*-carbon and *W*-carbon with the corresponding strain at which the maximum stress (GPa) occurs.

	Z-carbon		*W*-carbon	
Deformation	Stress	Stain	Stress	Stain
[001]	127.5	0.25	112.7	0.18
[010]	71.4	0.12	110.8	0.25
[100]	91.4	0.14	83.9	0.17
[011]	86.6	0.13	97.8	0.16
[101]	96.2	0.16	68.8	0.13
[110]	97.7	0.15	86.8	0.17
[111]	102.2	0.17	72.0	0.13

Table V. Calculated ideal shear strength for *Z*-carbon and *W*-carbon with the corresponding strain at which the maximum stress (GPa) occurs.

Z-carbon			*W*-carbon		
Deformation	Stress	Stain	Deformation	Stress	Stain
(010)[100]	87.2	0.28	(100)[001]	67.8	0.19
(010)[001]	99.9	0.27	(100)[010]	96.6	0.29
(010)[101]	87.5	0.29	(100)[011]	72.6	0.21
(001)[100]	109.3	0.27	(001)[100]	75.6	0.19
(001)[010]	104.5	0.28	(001)[010]	90.1	0.22
(001)[110]	108.6	0.27	(001)[110]	83.0	0.21
(100)[001]	103.1	0.27	(101)[010]	100.7	0.28
(100)[010]	93.1	0.29	$(101)[10\bar{1}]$	63.8	0.18
(100)[011]	100.0	0.29	$(101)[11\bar{1}]$	62.1	0.16

Table VI. Calculated frequencies ω (cm^{-1}) of the Raman modes for *Z*-carbon, *W*-carbon, *M*-carbon and bct-C_4 carbon, respectively.

Z-carbon		*W*-carbon		*M*-carbon		bct-C_4	
Mode	ω	Mode	ω	Mode	ω	Mode	ω
B_g	525.5	B_{3g}	426.9	B_g	329.8	E_g	492.0
A_g	570.7	A_g	429.9	A_g	362.9	B_{2g}	788.0
B_g	671.2	B_{2g}	664.1	A_g	492.4	B_{1g}	1036.7
A_g	916.3	B_{1g}	686.3	B_g	656.8	A_{1g}	1055.0
A_g	987.7	A_g	897.7	B_g	685.7	B_{1g}	1086.6
A_g	1063.0	A_g	909.5	B_g	716.6	E_g	1287.4
A_g	1187.6	B_{2g}	917.3	A_g	784.8	B_{2g}	1291.1
A_g	1194.2	B_{2g}	1002.0	A_g	881.1	A_{1g}	1350.5
B_g	1259.5	B_{1g}	1041.5	A_g	917.3		
B_g	1291.9	A_g	1087.8	A_g	948.6		
A_g	1300.6	B_{3g}	1133.8	A_g	1005.2		
A_g	1328.5	B_{2g}	1141.1	A_g	1052.9		
		B_{1g}	1195.4	B_g	1137.7		
		B_{2g}	1238.1	B_g	1204.6		
		B_{3g}	1243.7	A_g	1222.0		
		A_g	1253.0	B_g	1248.1		
		B_{2g}	1258.5	A_g	1254.9		
		A_g	1270.4	A_g	1255.9		
		A_g	1285.5	A_g	1279.2		
		B_{2g}	1294.7	A_g	1291.4		
		B_{1g}	1340.3	A_g	1318.7		
		B_{3g}	1346.6	A_g	1325.0		
		A_g	1398.7	B_g	1341.8		
		B_{2g}	1411.9	A_g	1414.7		

Table VII. Calculated frequencies ω (cm^{-1}) of the optic IR modes for *Z*-carbon, *W*-carbon, *M*-carbon and bct-C_4 carbon, respectively.

Z-carbon		*W*-carbon		*M*-carbon		bct-C_4	
Mode	ω	Mode	ω	Mode	ω	Mode	ω
A_u	679.9	B_{3u}	366.4	B_u	405.1	E_u	1016.7
B_u	783.5	B_{1u}	473. 4	A_u	425.5	E_u	1035.8
B_u	988.3	B_{1u}	520.5	B_u	484.7	A_{2u}	1160.7
B_u	1010.5	B_{2u}	567.1	A_u	565.7	E_u	1240.3
B_u	1081.5	B_{2u}	668.6	B_u	666.8		
A_u	1134.0	B_{3u}	751.5	A_u	668.4		
B_u	1242.5	B_{1u}	852.0	B_u	769.0		
B_u	1303.4	B_{3u}	945.9	B_u	906.1		
A_u	1333.0	B_{1u}	968.8	B_u	938.2		
		B_{3u}	1062.1	B_u	1028.9		
		B_{1u}	1102.7	A_u	1039.6		
		B_{3u}	1141.5	A_u	1057.0		
		B_{2u}	1206.2	B_u	1118.6		
		B_{3u}	1268.6	B_u	1148.3		
		B_{3u}	1280.9	B_u	1159.5		
		B_{1u}	1282.9	A_u	1205.3		
		B_{1u}	1299.3	B_u	1249.2		
				B_u	1282.5		
				B_u	1295.3		
				A_u	1338.9		
				B_u	1400.1		

Figures and Figure Captions

FIG. 1 (color online) Calculated tensile stress versus tensile strain for *Z*-carbon, *W*-carbon in principal symmetry directions compared to those of *M*-carbon, bct-C_4 and diamond.

FIG. 2 (color online) Calculated shear stress versus shear strain for *Z*-carbon and *W*-carbon in principal symmetry directions compared to those of *M*-carbon, bct-C_4 and diamond.

FIG. 3 (color online) The calculated contour slices of ELF of *Z*-carbon at equilibrium (S0) and at strain 0.28 (S1) and 0.3 (S2) during shearing along the (010)[100] path and *W*-carbon at equilibrium (S0) and at strain 0.16 (S1) and 0.17 (S2) during shearing along the $(101)[11\bar{1}]$ path.

FIG. 4 (color online) The C-C bonds connected with carbon squares viewed along (001) direction (*a*), and Viewed along (010) direction (*b*) for *Z*-carbon.

FIG. 5 (color online) The conventional unit cell of *Z*-carbon (*a*) and *W*-carbon (*b*) with bonding hardness values and ELF isosurface with the ELF value of 0.75, respectively.

FIG. 6 Calculated phonon dispersion curves and the density of states (DOS) for *Z*-carbon (*a*) and *W*-carbon (*b*) under pressures of 0 GPa and 300 GPa, respectively.

FIG. 7 Simulated Raman spectra for *Z*-carbon(*a*), *W*-carbon(*b*), bct-C_4(*c*), and *M*-carbon(*d*) at 0 GPa, respectively.

FIG. 8 Simulated IR spectra for *Z*-carbon(*a*), *W*-carbon(*b*), bct-C_4(*c*), and *M*-carbon(*d*) at 0 GPa, respectively.

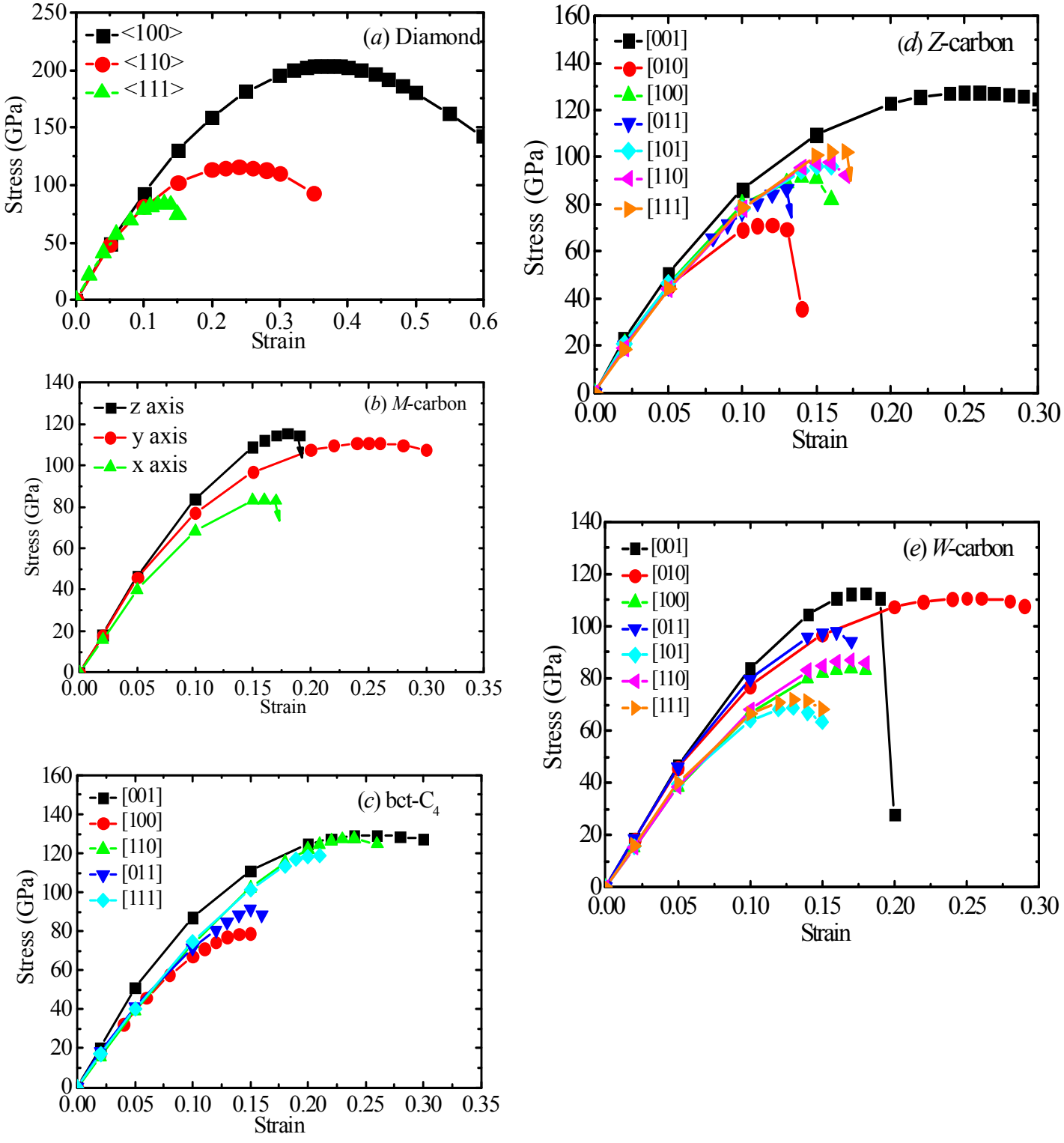
(a) Diamond
<100>
<110>
<111>
Stress (GPa)
Strain
(b) M-carbon
z axis
y axis
x axis
Stress (GPa)
Strain
(c) bct-C4
[001]
[100]
[110]
[011]
[111]
Stress (GPa)
Strain
(d) Z-carbon
[001]
[010]
[100]
[011]
[101]
[110]
[111]
Stress (GPa)
Strain
(e) W-carbon
[001]
[010]
[100]
[011]
[101]
[110]
[111]
Stress (GPa)
Strain

Fig. 1. Li *et al.*

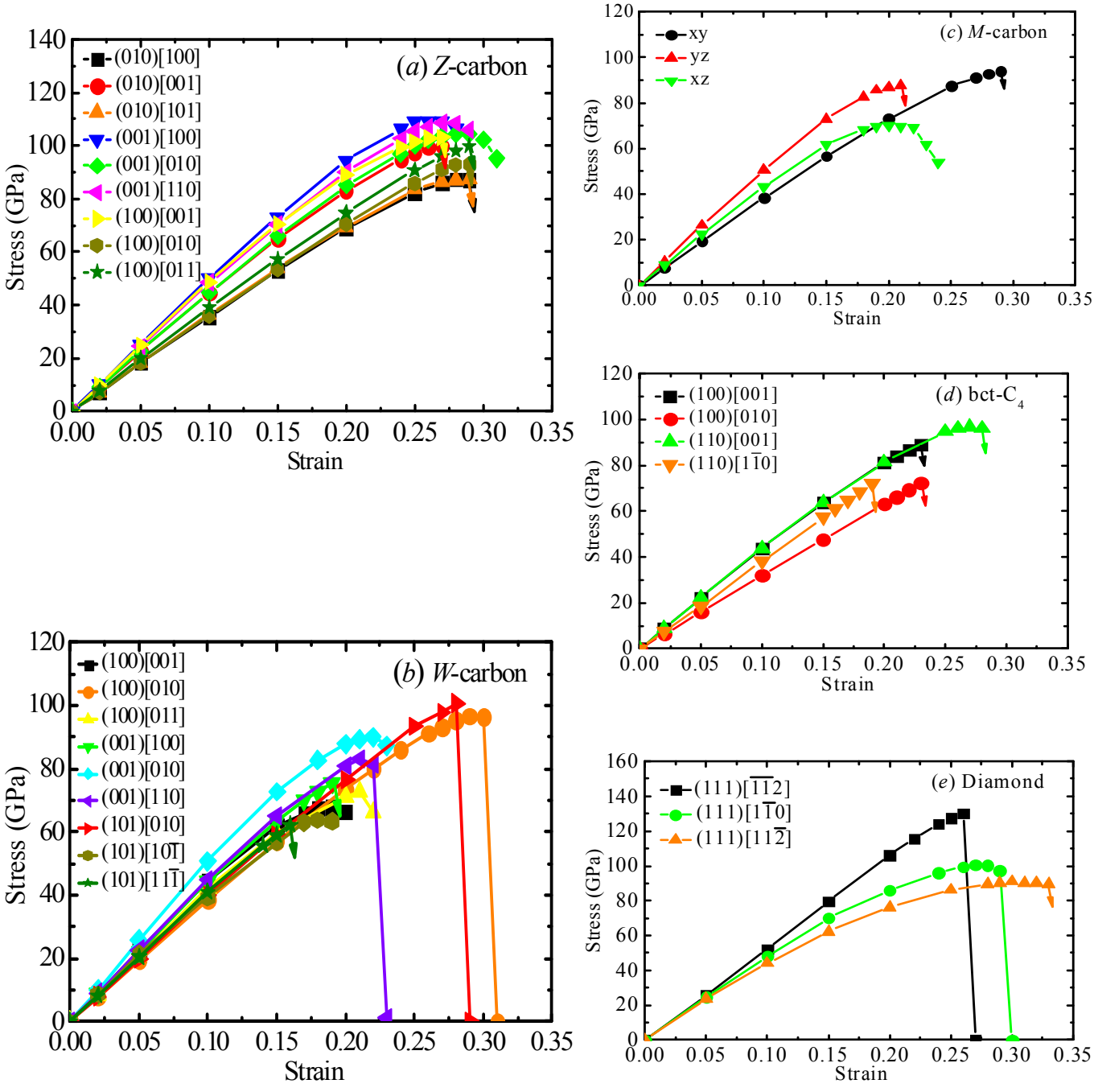
(a) Z-carbon
(010)[100]
(010)[001]
(010)[101]
(001)[100]
(001)[010]
(001)[110]
(100)[001]
(100)[010]
(100)[011]
(b) W-carbon
(100)[001]
(100)[010]
(100)[011]
(001)[100]
(001)[010]
(001)[110]
(101)[010]
(101)[10$\bar{1}$]
(101)[11$\bar{1}$]
(c) M-carbon
xy
yz
xz
(d) bct-C$_4$
(100)[001]
(100)[010]
(110)[001]
(110)[1$\bar{1}$0]
(e) Diamond
(111)[$\bar{1}\bar{1}$2]
(111)[1$\bar{1}$0]
(111)[11$\bar{2}$]
Stress (GPa)
Strain

Fig. 2. Li *et al.*

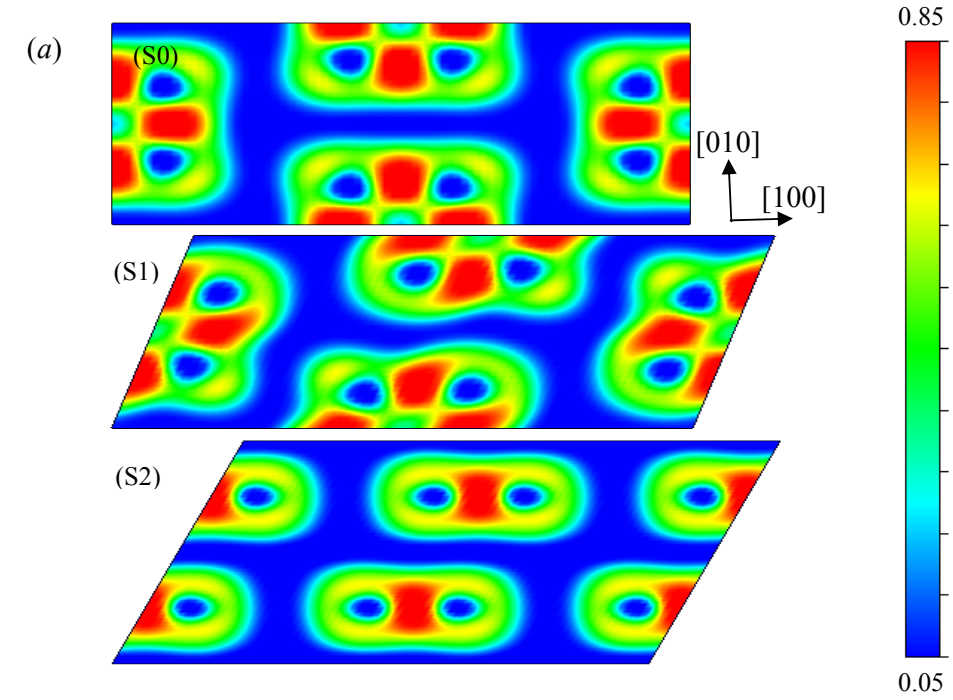

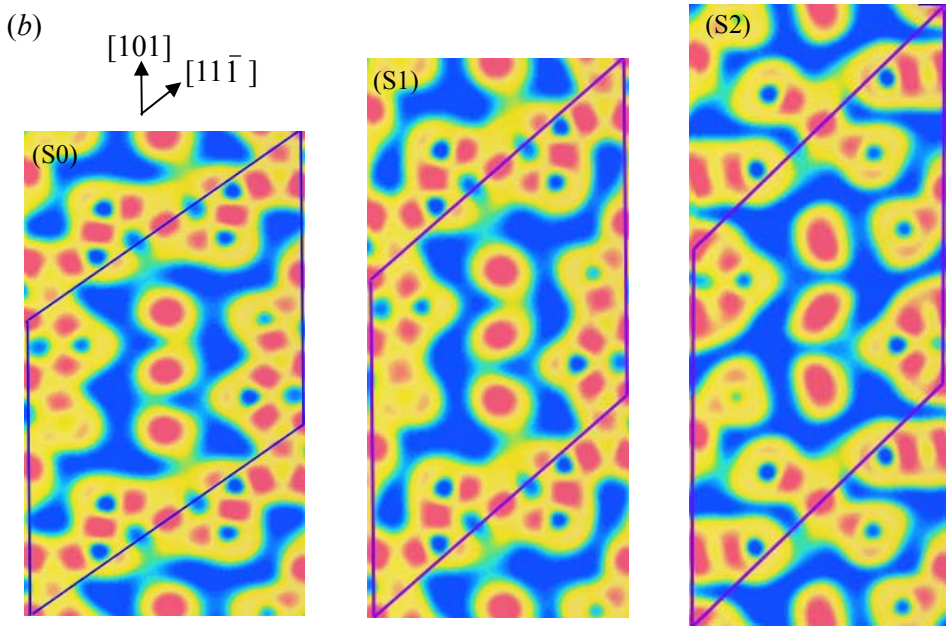

Fig. 3. Li *et al.*

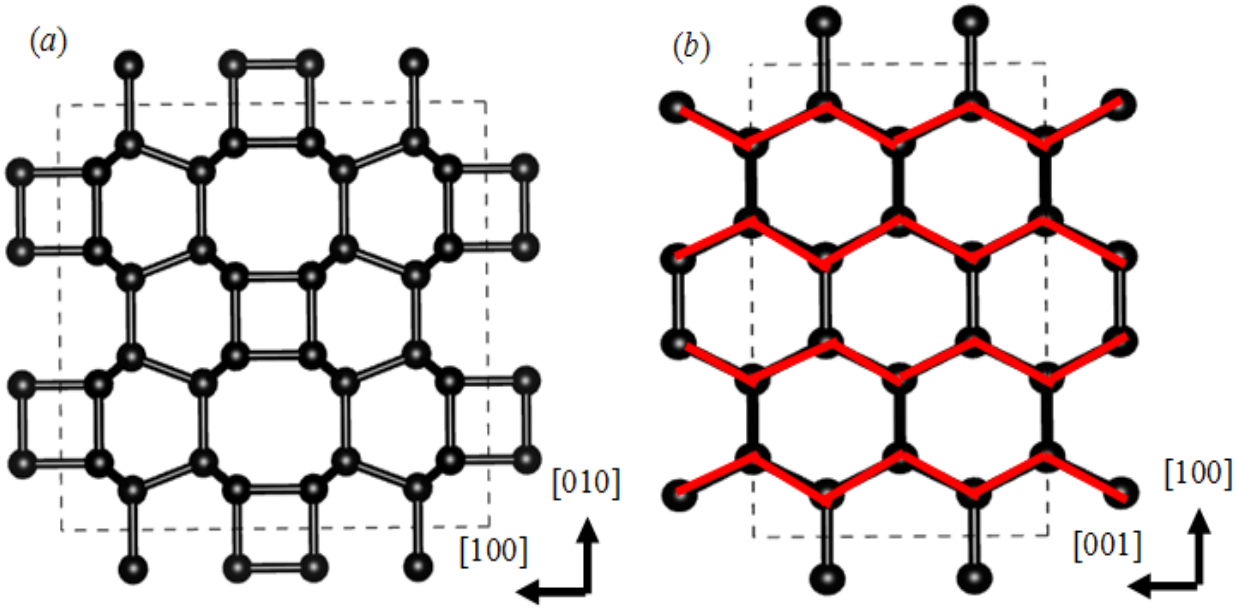

Fig. **4**. Li *et.al*.

(*a*)

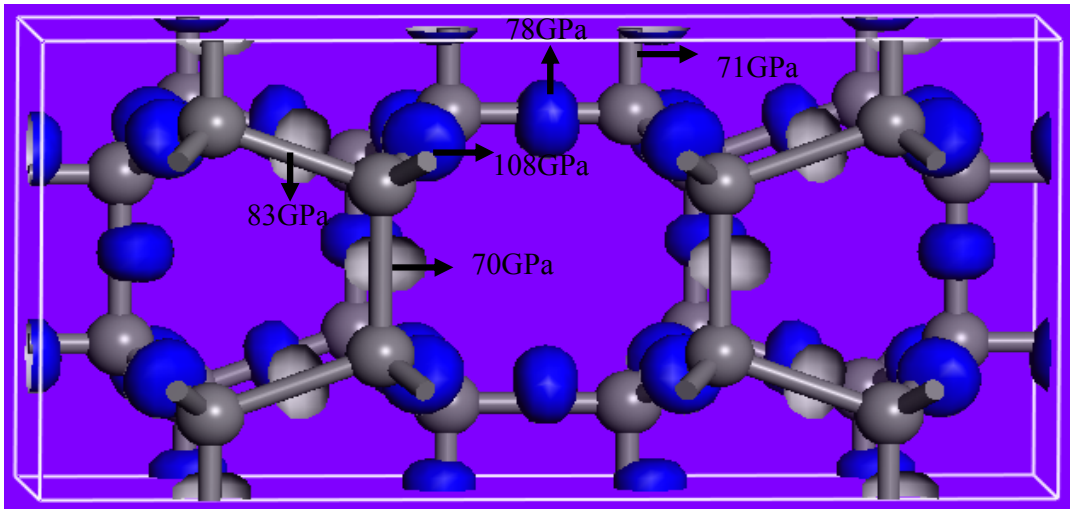

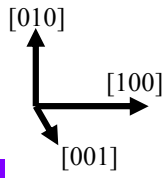

(*b*)

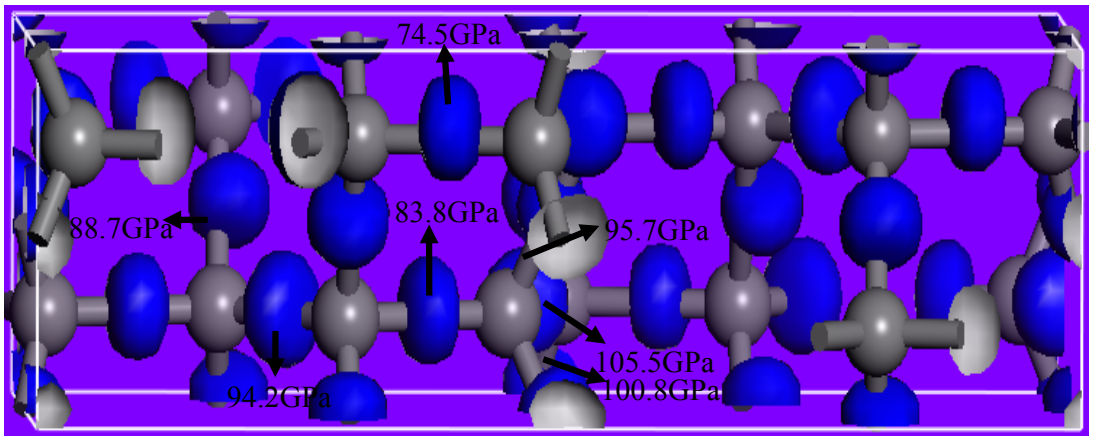

Fig. 5. Li *et al.*

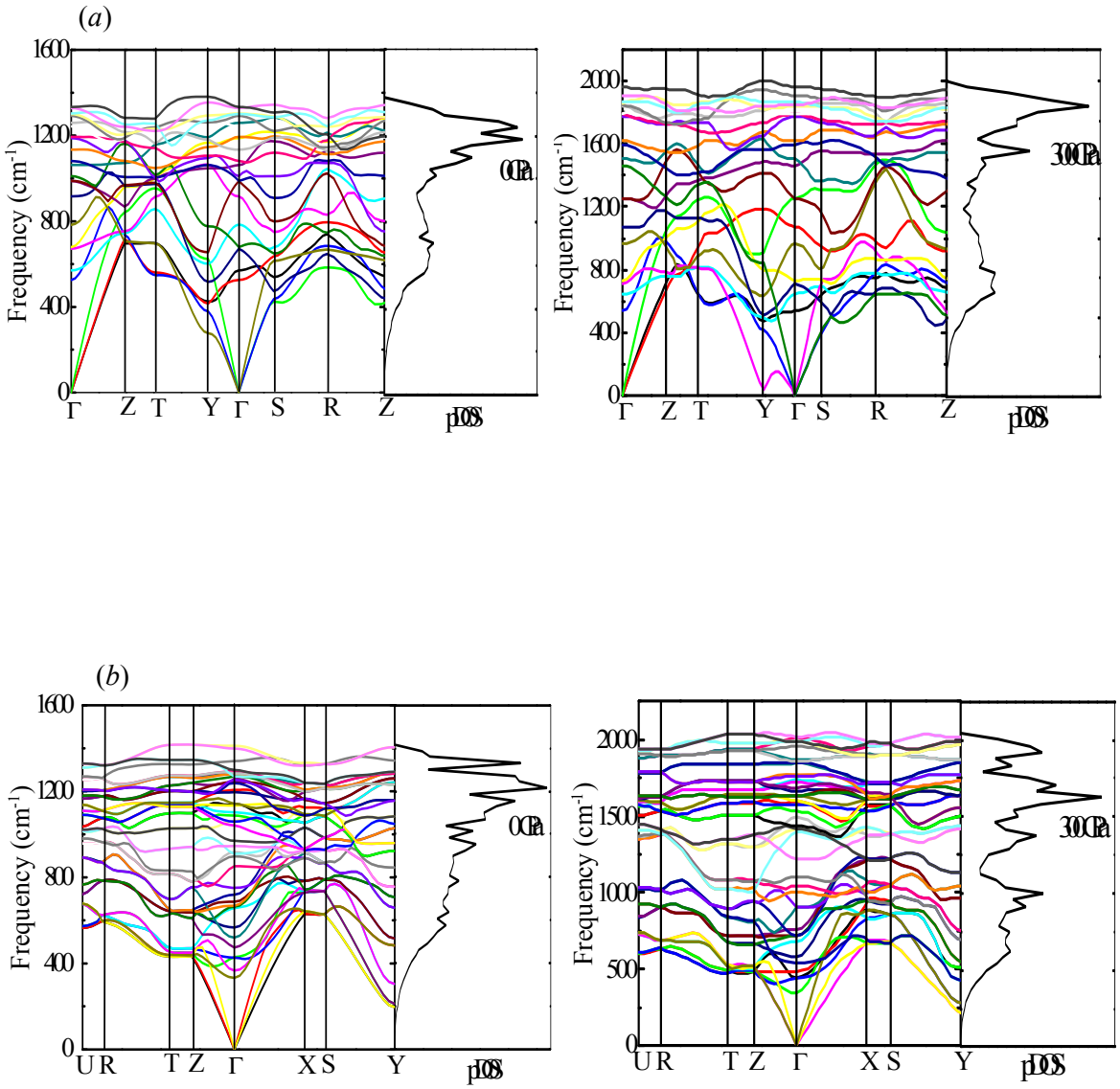

Fig. **6**. Li *et.al*.

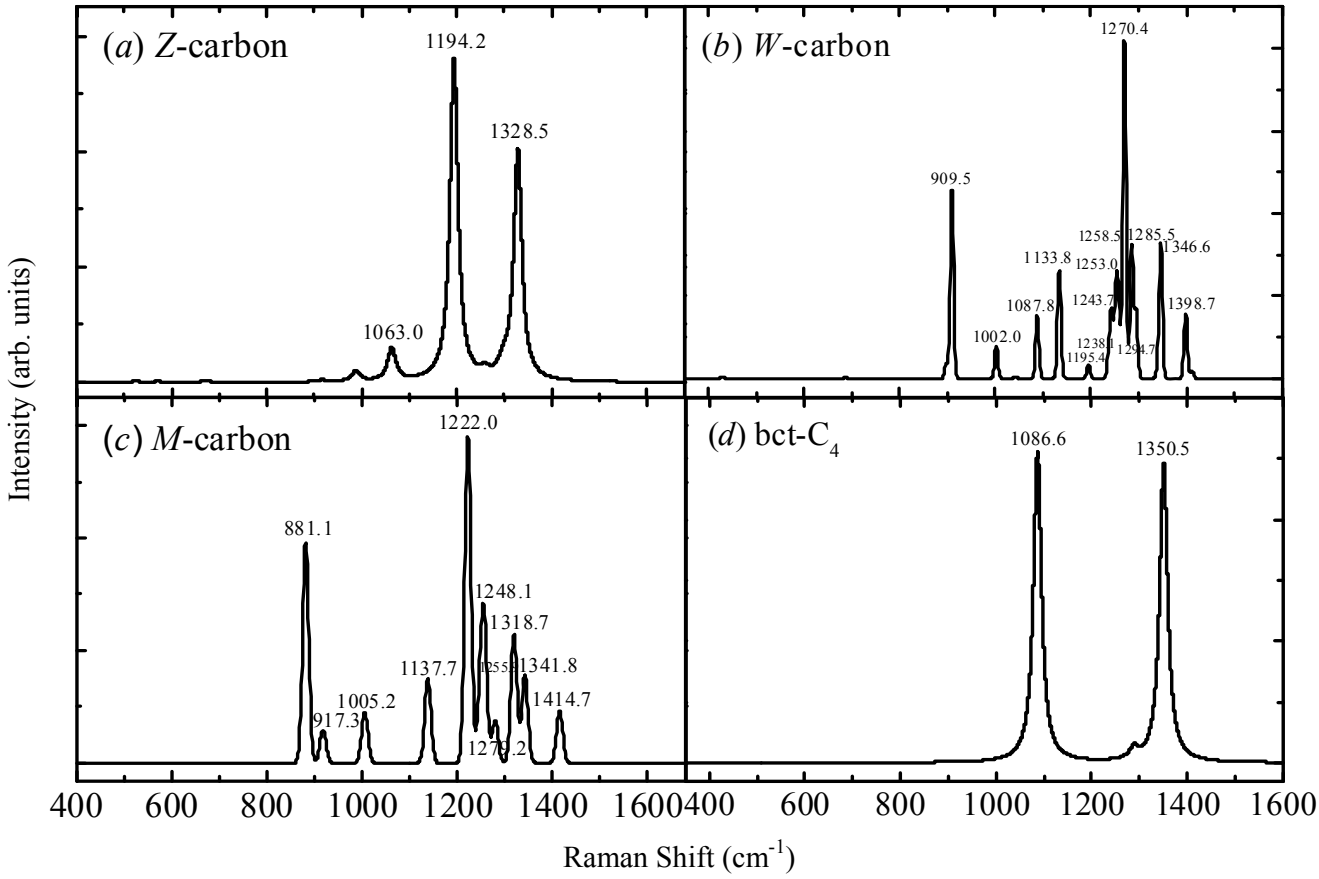
(a) Z-carbon
1194.2
1328.5
1063.0
(b) W-carbon
1270.4
909.5
1258.5
1285.5
1346.6
1133.8
1253.0
1087.8
1243.7
1398.7
1002.0
1238.0
1195.4
1294.7
(c) M-carbon
1222.0
881.1
1248.1
1318.7
1137.7
1341.8
1005.2
1414.7
917.3
(d) bct-C4
1086.6
1350.5
Intensity (arb. units)
400
600
800
1000
1200
1400
1600
Raman Shift (cm-1)

Fig. **7**. Li *et.al*.

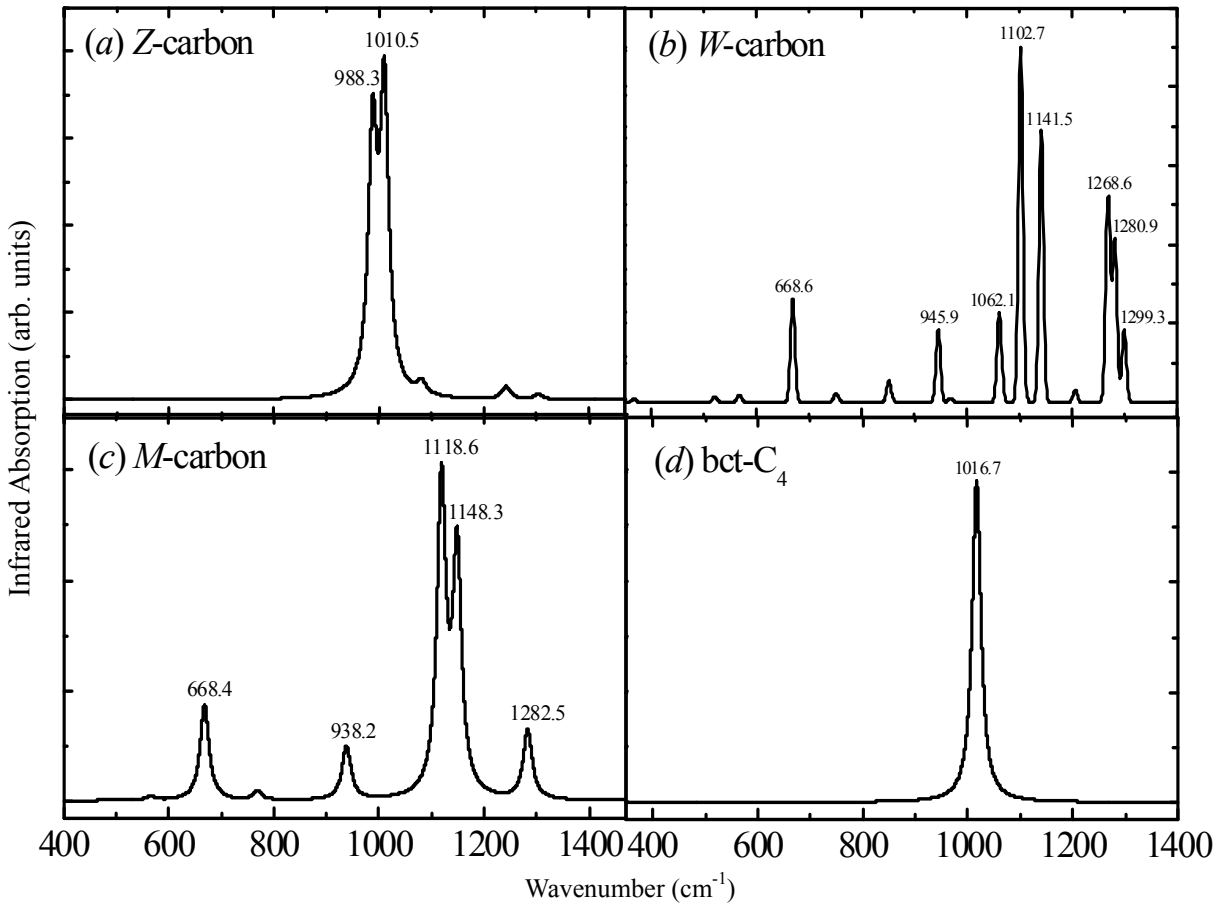
(a) Z-carbon
1010.5
988.3
(b) W-carbon
1102.7
1141.5
1268.6
1280.9
668.6
945.9
1062.1
1299.3
(c) M-carbon
1118.6
1148.3
668.4
938.2
1282.5
(d) bct-C4
1016.7
Infrared Absorption (arb. units)
400
600
800
1000
1200
1400
Wavenumber (cm-1)

Fig. **8**. Li *et.al*.